A VNA-Based Wideband Measurement System for Large-Signal Characterization of Multiport Circuits

A VNA-Based Wideband Measurement System for Large-Signal Characterization of Multi-Port Circuits

Christoph Schulze, Mattia Mengozzi, Gian Piero Gibiino, Alberto Maria Angelotti, Corrado Florian, Alberto Santarelli, Wolfgang Heinrich, Olof Bengtsson

***Abstract*—This work reports on a wideband (WB) measurement system based on a vector network analyzer (VNA) topology for multi-port large-signal measurements. The setup exploits a modified commercial VNA with WB intermediate frequency (IF) outputs that allows for more than 5 GHz analysis bandwidth (BW), where the IF is captured using an external high-speed oscilloscope. A three-port configuration using six receivers is described, together with the signal processing to achieve the high dynamic range required for WB signal measurements. The calibration procedure to establish reference planes at the three ports of the device-under-test (DUT) are shown. A comparison is made between single-tone continuous-wave (CW) calibration and WB calibration using multi-tone signals, illustrating advantages, challenges and limitations. The system is then demonstrated for on-wafer WB characterization and linearization of a Dual Input Doherty Power Amplifier (DIDPA) using a 100-MHz instantaneous BW excitation signal at millimeter-wave frequencies. By leveraging on the error-corrected WB waves, an algorithm is proposed for modulated input signal control across a 600-MHz acquisition BW at the DUT on-wafer reference planes. The algorithm enables a user-defined emulated splitting of the input WB signals. The linearization performance of such an emulated PA configuration is finally evaluated.**

***Index Terms*—Digital predistortion (DPD), doherty power amplifier (DPA), millimeter-wave measurements, vector network analyzer (VNA), wideband measurements.**

I. Introduction

MODERN applications of wireless telecommunications, as well as radar, exploit modulated signals at millimeter-wave frequencies with increasingly wider bandwidths (BWs), in the range of hundreds of MHz and beyond. Components and subsystems are therefore required to operate across large instantaneous BWs, so that instrumentation and characterization features need to be adapted to this demanding scenario. Nonlinear devices, such as radio-frequency (RF) power amplifiers (PAs), require network analysis to extract figures-of-merit (FoMs) like input and output match, available power gain, load-pull contours, etc. At the same time, they also require signal analysis FoMs like the error vector magnitude (EVM) [1]. As an additional complication, modern PA topologies addressing the ever-demanding trade-off between broadband linearity and power efficiency often result in complex modules with multiple ports and input signals [2]. This includes topologies like Doherty, envelope tracking and load-modulated circuits with active signal injection, where measurements need to be conducted at non-50-Ω interfaces. Considering the applications at millimeter-wave frequencies, such topologies are now being implemented as Microwave Monolithic Integrated Circuits (MMICs) with a requirement to measure the chip performance on-wafer, before dicing and placing the MMICs in multi-chip modules [3]–[5].

There are several receiver options for capturing wideband (WB) signals at millimeter-wave frequencies, each with their own pros and cons. One straightforward approach is to measure the time-domain RF signal directly with a high-frequency oscilloscope, given the availability of commercial solutions in the 70-GHz to 110-GHz range [6], [7]. However, the resolution can be poor, which does not generally facilitate reference plane calibration for non-50-Ω measurements [8]. Moreover, these solutions can become extremely expensive for multi-channel high-frequency measurements where numerous receivers are required.

The conventional method for characterizing relevant features of WB signals at high carrier frequencies is by utilizing spectrum analyzers in the frequency domain. FOMs based on spectral regrowth like adjacent channel power ratio (ACPR) or noise power ratio (NPR) can be readily measured in a 50-Ω environment. However, given the ever-growing trend toward complex modulation schemes, the addition of vector signal analysis tools beyond amplitude-only information have become necessary in millimeter-wave component testing. Built-in or external IQ demodulators allow for envelope-domain characterization, including dynamic amplitude-to-amplitude (AM/AM) and amplitude-to-phase (AM/PM) distortion analysis, as well as the generation of constellation diagrams with EVM. While modern vector signal analyzers (VSAs) can be used for standard-compliant performance with analysis BW of several GHz at carrier frequencies of up to 67 GHz [9], [10], even a single-receiver VSA system of this quality can be costly, and it is not suitable to account for impedance mismatch. In the latter case, it is necessary to establish reference planes and to measure the incident and reflected WB signal waves at each port in a vector network analyzer (VNA) configuration, which requires several receivers.

Legacy VNAs are mostly used for measuring scattering parameters by exploiting the high dynamic range provided by frequency-domain downconversion and narrowband receivers.

They readily allow for multi-port reference planes definition and vector error correction for relative quantities. More

This work was partly funded by the German Federal Ministry of Education and Research (BMBF) under the project reference 16FMD02 (Forschungsfabrik Mikroelektronik Deutschland).

C. Schulze, W. Heinrich and O. Bengtsson are with Ferdinand-Braun-Institut, Leibniz-Institut fuer Hoechstfrequenztechnik, Gustav-Kirchhoff-Str. 4, 12489 Berlin, Germany (email: christoph.schulze@fbh-berlin.de).

M. Mengozzi, G. P. Gibiino, A. M. Angelotti, C. Florian and A. Santarelli are with DEI "G. Marconi", University of Bologna, Viale Risorgimento 2, 40136 Bologna, Italy

recently, the range of available functionalities have been significantly expanded in the context of combined low- and high-frequency large-signal measurements [11]–[13], multi-port large-signal setups [14], [15], as well as WB signal analysis [16]–[23]. In [14], a calibrated multiharmonic setup is implemented for the characterization of a single-input dual-output PA. This configuration utilizes a switched receiver based on harmonic sampling for continuous-wave (CW) measurements. In [15], a switched configuration based on a four-port Large-Signal Network Analyzer (LSNA) makes use of a sequential two-port calibration for CW characterization of an outphasing PA. Solutions have been proposed for measuring the EVM of two-port [17], [18] or frequency converting devices [20], [22] on the basis of spectral correlations from relative acquisitions and absolute power measurements in the frequency domain.

While the inherent narrow IF BW of VNAs is typically insufficient for modern modulation BWs, techniques for measuring parts of the signal separately and then stitch them together with preserved phase and amplitude for the full-BW response have also been proposed [21]. These systems can make use of the built-in calibration features of the VNA system but need workarounds to handle the wide BW and to overcome the limited access to the internal hardware for timing and triggering [24].

Vector-correction and the definition of reference planes in these platforms enables signal analysis combined with WB load-pull [1], [16], as well as related algorithms for the emulation of load modulation [25].

In this work, an alternative VNA-based WB multiple-input multiple-output (MIMO) system is presented. It uses the general architecture of a mixer-based VNA yet modified to feature wideband IF outputs, which allow for the use of external digitizers to capture the full modulation BW. Coherent averaging is exploited to obtain the required dynamic range and vector error correction is implemented to establish reference planes for non-50-Ω measurements. This work extends the research presented in [26] by providing a more comprehensive description of the measurement system and by conducting a detailed investigation into the limiting effects on the overall system performance. The poor isolation of the mixer switch and of the local oscillator (LO) during calibration are investigated and shown to be responsible for the discrepancies between the CW and WB calibration reported in [26]. Furthermore, the WB IF acquisition based on the external oscilloscope is examined in detail, revealing the effects and limitations of intermodulation distortion (IMD), interleaving, and quantization.

The system is then demonstrated for the characterization of an on-wafer dual-input Doherty PA (DIDPA) operating at 24 GHz. Different from classical Doherty PAs with a passive input splitter, the main and the auxiliary (or peaking) amplifier branches of a DIDPA feature independent RF inputs, hence creating a three-port device. The tuning of the two inputs, just as for other dual input PA topologies [27], [28], allows for high adaptability of the PA operating conditions and improved efficiency [29], [30].

Several works have reported on the testing and linearization of DIDPAs, where the selection of the input splitting parameters is typically based on CW characterization [21], [31].

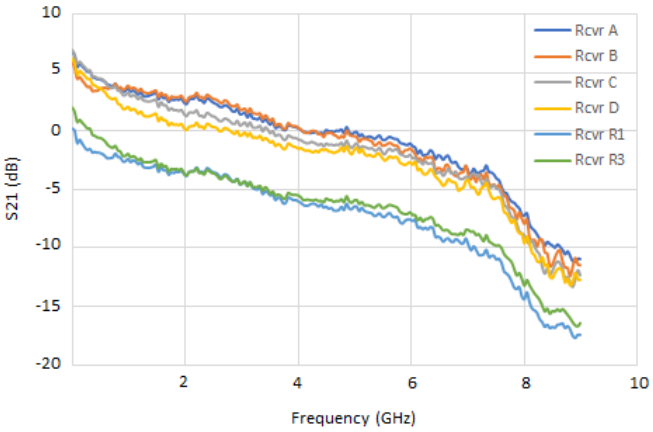

Fig. 1. Gain measurements of the modified PNA-X internal downconversion mixers plotted over the IF range. The characterization is obtained with RF excitation swept from 1.01 GHz to 10 GHz with a power level of -20 dBm. The LO is fixed at 1 GHz with a power level of 6 dBm.

In [32], the iterative learning control (ILC) has been used for DIDPA signal separation, but the proposed algorithm is based on preliminary static tests. In [33], the dual-input control strategy is implemented based on a model for the peaking amplifier. In [34] and [2], optimization techniques are investigated. In none of these cases, signal control is implemented at the calibrated device under-test (DUT) reference planes, as required for on-wafer MMIC testing at millimeter-wave frequencies. The work in [35] reports on a calibration technique based on a passive device for multi-port phase-coherent signal generation at a given reference plane, along with the CW characterization of a Load Modulated Balanced Amplifier (LMBA).

In this work, we present an algorithm to implement WB control at the calibrated DUT reference planes, directly using modulated excitations and without any preliminary characterization data. This allows for setting a user-defined WB input split for the DIDPA, and it allows selecting the optimum operating point under WB modulation. In addition, the technique is integrated in a nested loop to perform DUT linearization.

The article is organized as follows. The measurement system and related calibration are described in Section II and Section III, respectively. Section IV presents the procedure for WB multiple input signal control required to establish coherent waves with given phase and amplitude relationships at the calibrated reference planes. Section V reports on the DIDPA case study. Finally, a summary and outlook is given in Section VI.

II. Measurement System

A. General System Configuration

The core of the WB measurement system is a modified 4-port PNA-X VNA (Keysight N5247BC). One modification is the upgraded mixers for WB IF downconversion enabling an IF BW that exceeds 6 GHz, as shown in Fig. 1. For this work, it has been limited to 600 MHz, fully covering the

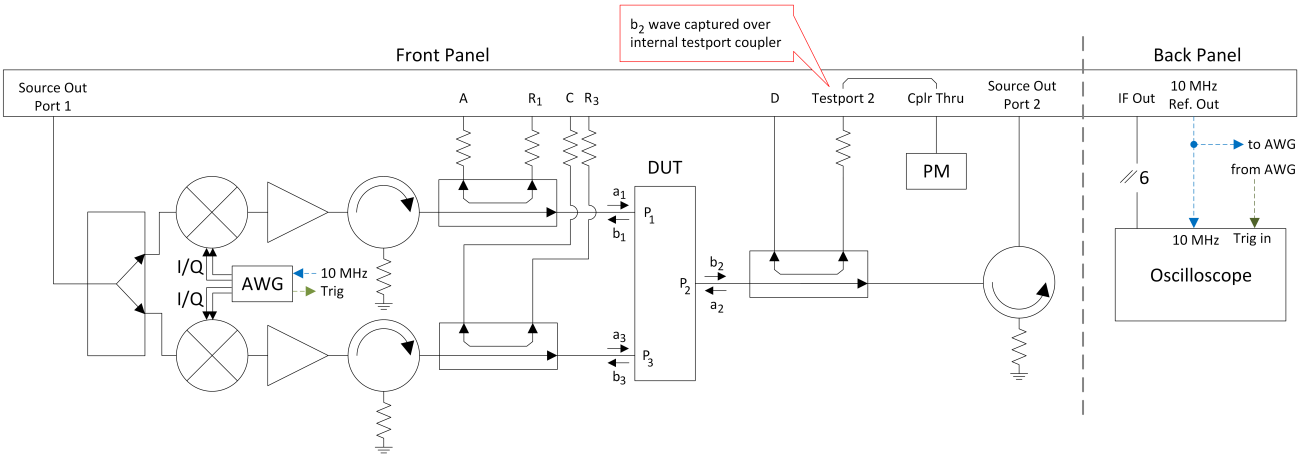

Fig. 2. Block diagram of the three-port wideband measurement system based on the PNA-X.

3rd and 5th order distortion for the 100-MHz BW excitation signal in use for DUT characterization (see Section V). The block diagram of the complete setup is shown in Fig. 2, while its photo is shown in Fig. 3. Six of the eight receivers, all apart from receiver 2 (R_2) and receiver 4 (R_4), are available at the back-plane of the PNA-X for external use. In this implementation, these six WB-IF signals are captured with a 6-GHz multi-channel oscilloscope (Keysight MXR608A). The three-port measurements reported in this work make use of WB receivers for all waves. The incident wave at port 2 (a_2), normally captured with R_2, is re-routed to the WB receiver D. The external test-set includes three pairs of 50-GHz directional couplers for the incident and reflected waves at all reference ports 1 to 3 (P_1, P_2, and P_3, respectively). Attenuator pads are used to optimize the dynamic range of the system up to a maximum 10-W peak power. The modulated signals are generated using two IQ mixers (Marki Microwave MMIQ-1040L), with the LO fed from the PNA-X. A Tabor WX2184C arbitrary waveform generator (AWG) is used to generate the baseband signals, and also to provide the trigger for synchronizing the acquisitions for WB measurements. All instruments run on a common 10-MHz reference. The DUT input ports P_1 and P_3 are equipped with isolated pre-amplifiers providing enough input power to saturate the DUT, while P_2 is terminated in a circulator and passive load. The coupled reflected wave b_2 is also routed through the internal PNA-X back-plane to a power meter for WB power measurements. This symmetrical build facilitates future extension of the system for active load-pull and load-modulated measurements in general. The present system is configured to operate at 24 GHz and the RF hardware limits the useful BW to 600 MHz. For an adapted RF configuration or for realizing a wider BW the maximum analysis BW using a single band WB calibration is 1.15 GHz, as limited by the AWG. With CW calibration, the analysis BW of the IF section exceeds 5 GHz.

B. IF configuration

The IF signals are coherently captured with 10-bit resolution at a sampling rate of 8 GS/s over 80k samples, corresponding to a frequency resolution of 100 kHz. The oscilloscope is triggered from the reference receiver channel of the active port and performs acquisition with an averaging factor of 1000, reducing the noise floor of about 30 dB compared to the case without averaging. With this procedure, a signal-to-noise ratio (SNR) exceeding 85 dB was measured as shown in Fig. 4. To achieve the maximum dynamic range of the oscilloscope channels, auto-scaling was used just once at the beginning of each receiver measurement. To avoid clipping, a margin was added to the auto-scaling of the scope. With this approach, different frequency points are measured using different ranges of the oscilloscope, causing different levels of quantization noise. For signals that are captured at lower resolution, the quantization noise becomes more significant relative to the carrier amplitude.

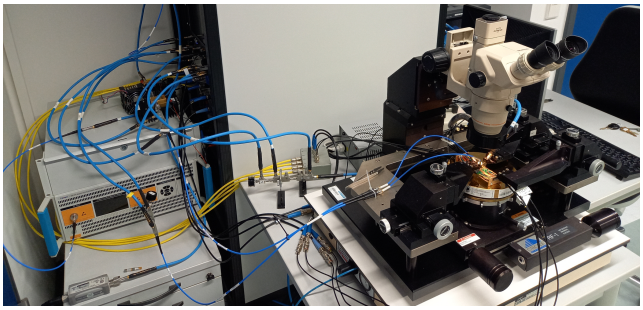

Fig. 3. Photo of the measurement setup at the FBH.

Channel scaling also affects the absolute power of the ADC interleaving spurs, which appear due to path-length differences and sample clock jitter. For the used oscilloscope, the interleaving spurs were determined by changing the vertical resolution without applying any input signal to the channels. They appear at multiples of 400 MHz, which are marked in red in Fig. 4. The power level of the spurs increases about 50 dB between minimum and maximum vertical resolution of the oscilloscope. The CW calibration over 600 MHz starting at 100 MHz IF crosses the spur at 400 MHz, which can reduce the quality of the calibration especially regarding the phase. For an optimum vertical scaling of the oscilloscope in this particular frequency point, the power of the spur is very low

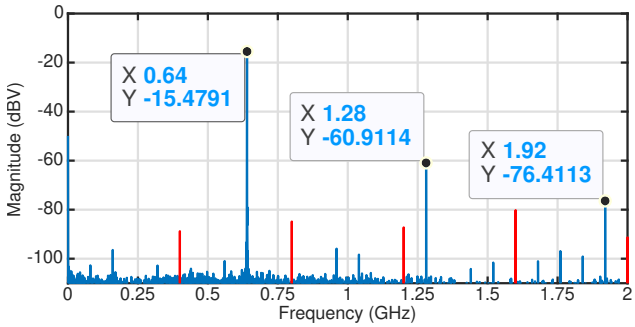

Fig. 4. Reference receiver R_3 spectra at load calibration for a downconverted input signal at 640 MHz. Higher order harmonics labeled and interleaving spurs at multiple of 400 MHz marked in red.

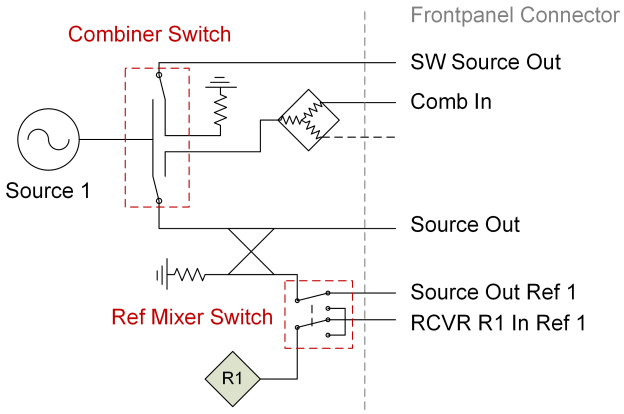

Fig. 5. Internal signal path of the PNA-X with combiner and mixer switch.

and its influence is negligible.

C. Isolation of internal PNA-X Switch and External Mixers

The setup shown in Fig. 2 makes use of the PNA-X Source 1 and an external power splitter to feed a common coherent LO for the external mixers for P_1 and P_3. The source signal is coupled by the internal coupler and terminated at the *Source Out Ref1* front panel connector while the reference mixer switch was set to external path as shown in Fig. 5. However, the reference mixer switch has very poor isolation and leads to a leaked LO signal at receiver 1 (R_1) with an amplitude ripple of more than ± 0.5 dB, affecting the quality of the calibration during the forward transmission/reflection measurements of P_1 or P_3. In order to avoid this, the LO signal can instead be directly fed to the PNA-X *SW Source Out* front-panel connector through the combiner switch, allowing for more power compared to the regular *Source Out* path. The internal coupler is then left unused and does no longer contribute with any leaked signals to R_1.

For the full three-port calibration, the sources of all ports (except for that of the active port) should be sequentially turned off. The injected power of the signals at P_1 and P_3 can be controlled through the IQ-mixers. The maximum isolation between the ports can be achieved by increasing the amplitude of the IQ input signals on one mixer while disabling the corresponding AWG outputs for the IQ input signals on the other mixer. A typical 47-dB LO-RF isolation

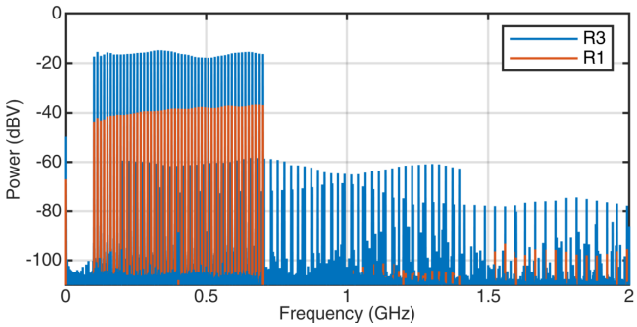

Fig. 6. Port 3 spectrum of R_3 (blue) and R_1 (red) receivers during the stepped CW reflection measurements of the load standard. Since multiple overlapping measurements are reported, the 2nd- and 3rd-order harmonics of the CW signals are visible as well and convey the impression of an in-band distortion, but it is just a visual effect.

is specified for the mixers used in this setup [36]. However, the differences in gain between the two pre-amplifiers, which are always operating during calibration, can cause significant leakage at the supposedly turned-off port, thus decreasing the actual isolation. Increasing the IQ voltage of the mixers to improve the isolation during the calibration is limited by the power handling of the calibration standards in use. Indeed, the system in the presented configuration is configured for 10 W (40 dBm), while the calibration standards for the on-wafer calibration are rated for a maximum of 200 mW. Fig. 6 shows an example of the captured spectra of R_3 (blue) and R_1 (red) for the stepped CW load calibration of Port 3 (i.e., with power injected at P_3) for a 600-MHz BW around 24 GHz.

Beyond the power rating of the on-wafer standards, the IQ input power should be well below the 1-dB compression point of the IQ mixer to avoid intermodulation distortion (IMD) products overlapping on the frequency bins of the equally-spaced multisine excitation signal used for WB calibration. As the compression depends on the operating BW as well as on the LO power, a careful characterization of the mixers was performed under WB conditions using the unequally spaced multitone (USMT) signal technique proposed in [37]. As an example, Fig. 7 shows the measurement of an USMT signal for two different IQ input power levels, showing the IMD regrowth and the corresponding limitation in terms of usable dynamic range. To increase the isolation between P_1 and P_3, switches may be implemented in each branch to avoid amplification of the LO leakage.

III. System Calibration

A. CW-based Reference Plane Calibration

The measurements on the DUT were conducted on-wafer in a coplanar waveguide (CPW) probe-tip interface. In a first step, the path between the on-wafer P_1 reference plane and the power meter port was characterized. This includes two one-port calibrations: the first one as an on-wafer CPW calibration at P_1, and the second one as a coaxial calibration at the input of the directional coupler (intermediate reference plane) on the second port, with a thru-line placed between P_1 and P_2. The available source power was then corrected. It should be noted that, once the power meter is connected in its final position as

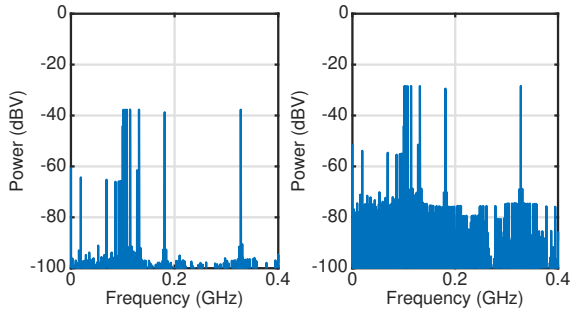

Fig. 7. Captured USMT signal at receiver R_3 in the presence of a load standard at P_3. The USMT features 9 generated tones between 100 MHz and 318.7 MHz using an IQ input voltage of 0.2 V (left) and 0.6 V (right).

in Fig. 2, the full path loss can be calculated without breaking any connections after calibration.

The reflection error terms, namely, the directivity errors (ED), source match errors (ES), and reflection tracking errors (ER) for each bin of the full measurement BW were then obtained by applying the short-open-load (SOL) procedure using a CW excitation, which enables SNR exceeding 85 dB as well as the identification of possible spurious signals generated by the internal PNA-X mixer bricks or by the oscilloscope receivers at IF [38]. Here, a 600-MHz band between 23.7 GHz and 24.3 GHz was calibrated at 601 frequency points (10-MHz spacing). The frequency offset mode of the PNA-X was used to maintain the LO of the internal PNA-X mixer bricks at $f_{LO} = 23.6$ GHz, resulting in a WB IF center frequency of 400 MHz, then stepping the CW frequency through all points to be calibrated.

The transmission error terms, namely, the transmission tracking errors (ET) and the load match errors (EL) were extracted from cross measurements of 4-ps thru-lines between P_1-P_2, P_3-P_2, and P_1-P_3, where the P_1-P_3 is a $180°$ bend structure. The measured calibration coefficients were then interpolated over intermediate bins for those signals with components that are not landing on the calibrated frequency grid. From the SOL and additional thru measurements, a total of 9 reflections error terms and 12 transmission error terms were extracted. These represents 5 of the 6 terms in the classical 6-term error box, where the leakage (cross-talk) terms are omitted.

Considering that the DUT is nominally matched at the inputs and output, only forward measurements with injected signals at P_1 and P_3 were here considered. Indeed, the load reflection as well as the system reflection within the measured BW have been verified to be negligible. Therefore, in this implementation, the power meter data was used together with the calibrated thru-line data to correct the relevant waves for absolute power. More general error models suitable for load-pull will be implemented in the future.

B. Verification using Wideband Excitation

The CW-based calibration procedure can become extremely time-consuming for a large number of calibration points, given that each frequency has to be set and captured multiple times

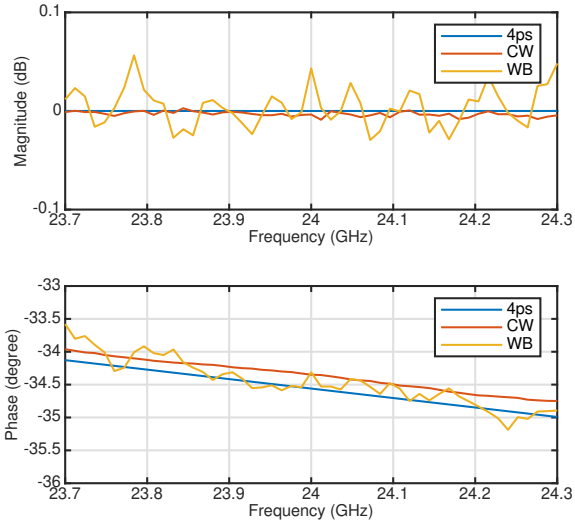

Fig. 8. Verification of magnitude and phase of a 4 ps thru line with stepped CW signal and 600 MHz Schroeder phased multisine signal over 51 frequency points.

for all three ports and calibration standards. The data acquisition for each frequency point is running inside a loop. It contains the capturing, examination for clipping, discrete Fourier transform and frequency selection since only one complex value is required for one specified frequency point. One pass of the loop takes approximately 3 seconds for a reflection and transmission standard measurement. An alternative and much faster solution is the calibration with a multitone WB signal. In particular, a Schroeder-phased multisine signal can be used to obtain a minimum crest factor [39]. To ensure the best possible dynamic range, the BW of the WB signal should be selected in order to avoid harmonic overlap. In this case, this was implemented by using 100-MHz WB excitation signals. Instead of measuring each standard for three ports over 601 sequential frequency points, only 6 measurements are required for one port and standard, enabling a substantial reduction in calibration time. In addition, coherent FFT filtering and stitching was performed in order to minimize the impact on the dynamic range of the IM products arising due to the non-linearity within the setup (e.g., compression of the external mixers).

In Fig. 8, the transmission measurement of a 4-ps thru line calibrated using the WB excitation across 600 MHz on 51 frequency bins is compared to the one obtained with a stepped CW signal as described in Section III-A. Overall, the WB measurement shows a slightly higher ripple in magnitude and phase, which can be ascribed to the overlapping IM products. The magnitude of such a ripple, however, is limited to less than ± 0.05 dB. The small offset in phase between the ideal and error-corrected thru line of less than 0.2 degrees at the CW verification are probably due to the manual probing and non-exact skating of the probe tips.

IV. Multiple-Input Wideband Signal Control

The nonlinear characterization of multi-port devices in the proposed stimulus-response environment requires customized control of the excitations to be applied to the DUT reference planes [35]. This work specifically targets the digital synthesis of the electrical conditions realized by a passive quadrature hybrid at the input of the DIDPA, emulating the behavior of a Doherty PA. The customized control of the two WB input signals allows to test the impact of different parameters of the hybrid splitter on the PA performance, without requiring any physical realization of the splitter circuit.

Without loss of generality, the quadrature hybrid will here be represented by imposing the condition $\mathbf{a}_3 = \alpha e^{j\phi}\mathbf{a}_1$, where α and ϕ are the splitting ratio and phase between the two inputs across the whole BW of interest. Various non-idealities in the signal path of each port (such as nonlinearity in the external mixers and pre-amplifies, as well as in the AWGs, or impedance mismatches) prevent, in general, the precise control of the actual waveforms at the DUT input reference planes. Therefore, even when specific α or ϕ values are imposed on the digital waveforms, different conditions might get realized at the DUT reference planes.

To both enforce the desired splitting conditions as well as linearize the resulting emulated PA, a nested algorithm based on ILC [40] is proposed. The digital input wave $\mathbf{a}_{1,d}$ to the main DIDPA branch at P_1 is initialized based on the target output modulated wave of interest $\mathbf{b}_{2,t}$ at P_2 as $\mathbf{a}_{1,d}^{(0)} = \frac{1}{G}\mathbf{b}_{2,t}$, where G is the chosen linearization gain. At the k-th iteration, the measurement of the output $\mathbf{b}_2^{(k)}$ wave is acquired, and the digital input signal $\mathbf{a}_{1,d}$ is updated using an outer ILC linearization loop:

$$\mathbf{a}_{1,d}^{(k+1)} = \mathbf{a}_{1,d}^{(k)} - \Gamma_1^{(k)}(\mathbf{b}_2^{(k)} - \mathbf{b}_{2,t}), \tag{1}$$

where $\Gamma_1^{(k)}$ is the learning gain at each iteration. For each iteration of this outer loop, the following inner ILC loop is used to impose the splitting conditions between the two inputs

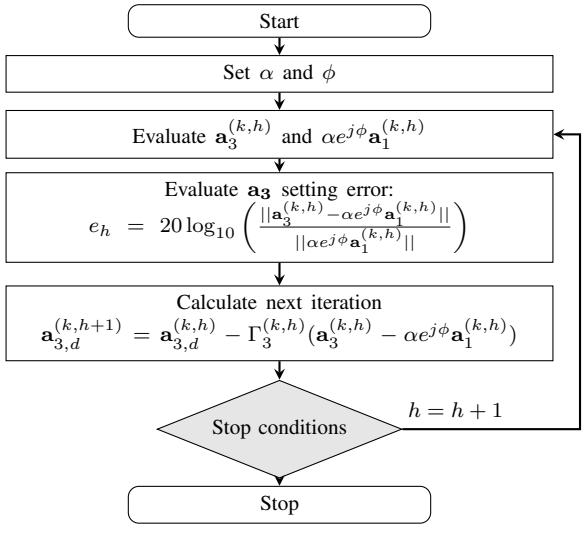

Fig. 9. Simplified flow chart of the ILC-based algorithm for dual input PA inner control loop.

by updating the input wave of the auxiliary branch $\mathbf{a}_{3,d}$ at P_3. That is initialized as $\mathbf{a}_3^{(k,0)} = \alpha e^{j\phi}\mathbf{a}_{1,d}^{(k)}$. Then, given that the initial conditions do not satisfy the target splitter emulation conditions at the DUT reference plane, iterative corrections are applied based on subsequent multi-port measurements, as depicted in the flow chart of Fig. 9. For this inner loop, the ILC algorithm is therefore run as follows:

$$\mathbf{a}_{3,d}^{(k,h+1)} = \mathbf{a}_{3,d}^{(k,h)} - \Gamma_3^{(k,h)}(\mathbf{a}_3^{(k,h)} - \alpha e^{j\phi}\mathbf{a}_1^{(k,h)}), \tag{2}$$

$\Gamma_3^{(k,h)}$ being the learning gain at each iteration of this inner loop. After convergence is reached for the inner loop, the two analog inputs $\mathbf{a}_1$ and $\mathbf{a}_3$ should satisfy the conditions imposed by the theoretical hybrid for the given α and ϕ values. Then, the outer ILC loop in (1) is stepped to the next iteration in order to linearize the PA output wave until the target $\mathbf{b}_{2,t}$ is reached.

V. Circuit Measurements

A. Device-Under-Test

The DUT is a DIDPA in MMIC technology designed in the WIN Semiconductors NP15-00 150-nm GaN-on-SiC process. It is centered at the carrier frequency of 24 GHz, achieving a gain of 25 dB by means of a two-stage topology. The driving stage of the DUT employs 2×75 μm High-Electron-Mobility Transistors (HEMTs), while the final stage uses 6×75 μm HEMTs for both the main and auxiliary PAs. The supply voltage for all stages of the DUT is 28 V.

B. DIDPA Linearization

Similarly to [21], a preliminary sweep of α and ϕ under CW excitation allowed to identify the specific input splitting values for obtaining the maximum power-added efficiency (PAE) at the given RF available input power of $P_{\text{AVS}} = 16$ dBm. This sweep resulted in the input splitting values ($\alpha = 1, \phi = -30°$), referred as **P0** in the following. In order to emulate this splitting behavior across the BW, these conditions are imposed by implementing the inner loop in (2). For this test, the DUT is excited by a random-phase multi-tone input test signal, whose statistics can be shaped to match 5G signals [18]. In particular, the excitation signal consists of 1k tones, covering a BW of 100 MHz and having a Peak-to-Average Power Ratio (PAPR) of 9.2 dB.

The red line in Fig. 10a corresponds to the injected wave $\mathbf{a}_1$ to the main branch of the DIDPA, while the blue line corresponds to the $\mathbf{b}_2$ wave after imposing the input splitting conditions **P0** without applying any linearization. The peak output power is $P_{\text{OUT}}^{\text{max}} = 29.3$ dBm, corresponding to more than 5 dB of compression. Figure 10b shows the iterative behavior of the inner loop for setting the selected input split. Figure 11 reports the same plots as Fig. 10 when applying DIDPA linearization, i.e., running both the outer loop in (1) and the inner loop in (2). The performance results in terms of ACPR, EVM, PAE, and average output power are reported in Table I for both cases (with and without linearization).

Figure 12 displays the corresponding behavior of the iterative normalized mean square error (NMSE) between $\mathbf{a}_3$ and

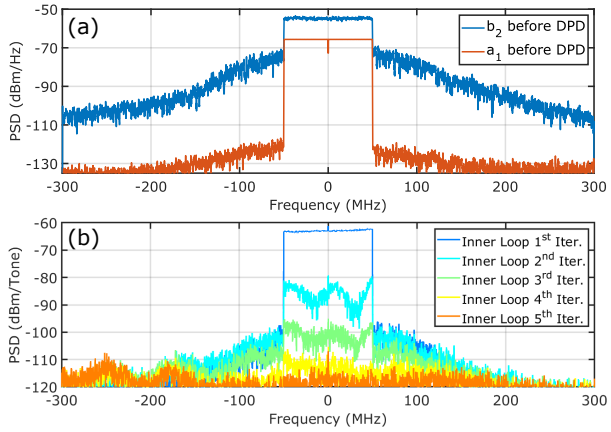

Fig. 10. DIDPA waves before linearization. (a) Spectra of $\mathbf{b}_2$ and $\mathbf{a}_1$. (b) Spectrum of iterative error $\mathbf{a}_3 - \alpha e^{j\phi}\mathbf{a}_1$ across the ILC-based inner loop.

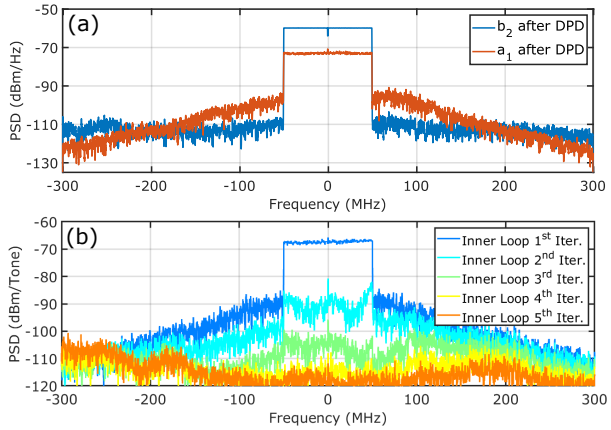

Fig. 11. DIDPA waves after linearization. (a) Spectra of $\mathbf{b}_2$ and $\mathbf{a}_1$ spectra. (b) Spectrum of iterative error $\mathbf{a}_3 - \alpha e^{j\phi}\mathbf{a}_1$ across the ILC-based inner loop.

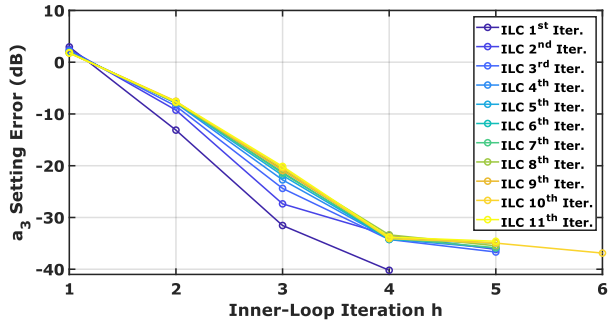

Fig. 12. Iterative behavior of the NMSE between $\mathbf{a}_3^{(k,h)}$ and $\alpha e^{j\phi}\mathbf{a}_1^{(k,h)}$ for dual input emulation (inner loop) and PA linearization (outer loop, color coding in the legend).

$\alpha e^{j\phi}\mathbf{a}_1$ (inner loop) across up to 11 iterations of the outer loop. It can be seen that, in all cases, the convergence (and hence, the user-imposed input signal splitting) can be achieved with an NMSE lower than -30 dB within four ILC iterations.

C. Selection of Input Splitting under Wideband Modulation

The dual input signal control and linearization techniques described in Section IV allow to identify optimum α and ϕ values directly under modulated conditions. Under a modulated regime, the resulting PAE is a weighted average across the instantaneous values of the output signal $\mathbf{b}_2$ i.e., the probability density function (pdf) of $\mathbf{b}_2$ acts as the weighting function, in general resulting in different PAE behavior and correspondingly different optimum values for α and ϕ. The resulting PAE under modulated conditions is shown in Fig. 13 for swept values of the splitting conditions, leading to the selection of two particular configurations for the digital splitter parameters, namely, **P1** ($\alpha = 0.5$ and $\phi = -30°$), found when the outer loop in (1) is not executed (i.e., without applying DIDPA linearization), and **P2** ($\alpha = 0.8$ and $\phi = -30°$), found when both the outer and inner loops are executed (i.e., applying DIDPA linearization).

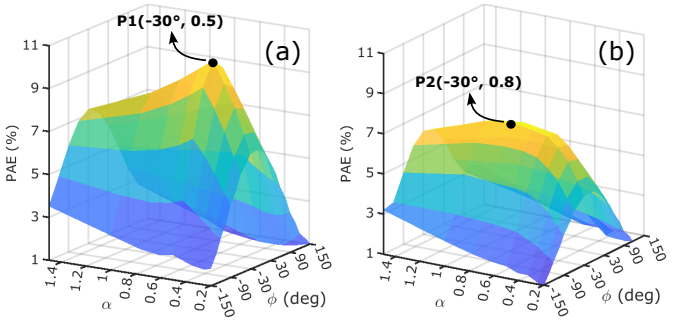

Fig. 13. PAE under modulated excitation for swept values of the input splitting conditions. (a) Without DIDPA linearization. (b) After DIDPA linearization.

TABLE I
DIDPA PERFORMANCE UNDER MODULATED EXCITATION AT DIFFERENT INPUT SPLITTING CONDITIONS.

FoM	**P0**	**P1**	**P2**
w/o linearization			
$P_{\text{OUT}}^{\text{rms}}$ (dBm)	25.4	23.2	21.7
PAE (%)	8.5	10.4	9.3
ACPR (dB)	-21.2	-26.3	-29.5
EVM (dB)	-15.7	-19.5	-20.4
w/ linearization			
$P_{\text{OUT}}^{\text{rms}}$ (dBm)	20.1	20.5	20.5
PAE (%)	7.2	7.1	7.4
ACPR (dB)	-48.8	-48.7	-50.7
EVM (dB)	-43.7	-39.2	-43.9

Then, regardless of how they were found, the input split settings as per **P1** and **P2** are imposed, with and without linearization, to evaluate the global performance of the DIDPA. The extracted FoMs are summarized in Table I, reporting the highest PAE in **P1** if no linearization is applied. On the other hand, when linearization is applied, a slightly higher PAE is obtained for **P2**. The measured dynamic gain and phase characteristics for the two operating points are reported in Figs. 14-15, while the spectra are shown in Fig. 16.

VI. Summary and Outlook

5G and space applications will require on-wafer WB characterization of multi-port nonlinear circuits at millimeter-wave frequencies. This experimental testing scenario involves the generation of several user-controlled coherent WB signals at power levels where system pre-amplifiers are likely to introduce non-linearities.

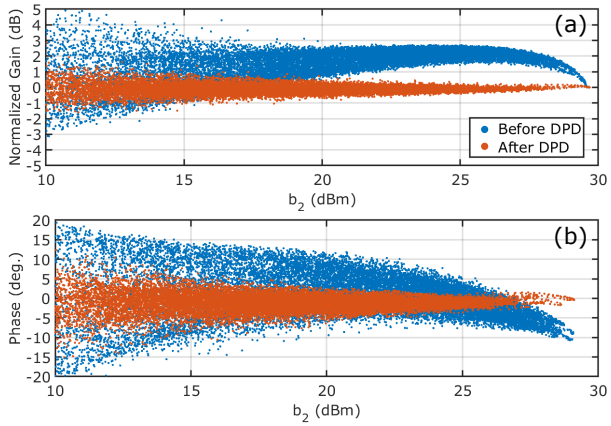

Fig. 14. Distorted and linearized (a) Gain and (b) phase characteristics of the DUT in the optimal point obtained without considering the effect of DPD on PAE (**P1**).

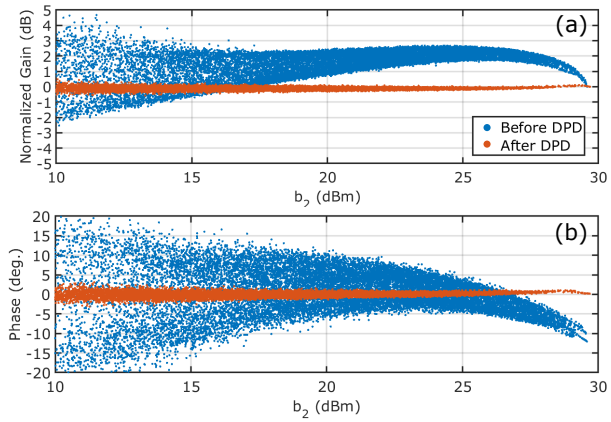

Fig. 15. Distorted and linearized (a) Gain and (b) phase characteristics of the DUT in the optimal point obtained considering the effect of DPD on PAE (P_2).

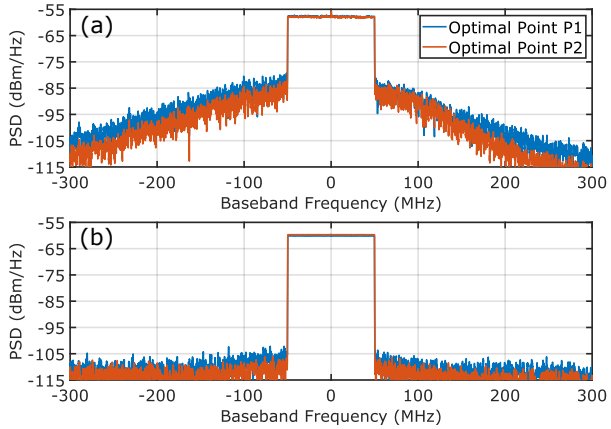

Fig. 16. Measured spectra of $\mathbf{b}_2$ at input splitting conditions **P1** and **P2** before (a) and after linearization (b).

This work presents a measurement system capable of measuring circuits across modulated BWs exceeding several GHz. It is based on a modified VNA used as a flexible source and downconversion mixer, where the downconverted WB IF is captured and analyzed externally in a real time WB oscilloscope. The setup, configuration, and calibration are presented with characteristics of the system including developed solutions to achieve the required measurement quality. CW-based calibration is compared to WB calibration and their advantages and disadvantages are discussed.

An iterative method to achieve control of the WB modulated signals at the DUT reference plane, thus correcting for the pre-amplifiers non-linearities, is presented. The calibrated system is then operated at millimeter-wave frequencies to explore the performance of a DIDPA under various emulated input splitting conditions.

This works shows the capabilities of the measurement system for a dual input Doherty amplifier, but the same setup can be used for other dual input RF amplifier system like out-phasing. The hardware setup is symmetrical with circulators on all ports and with a modified error model load modulated circuits can be measured with corrected injected signals on the output. Such a configuration would also enable the evaluation of reverse intermodulation and thermal coupling between the amplifiers in multiple PA array systems for beamforming by emulating the system reflections that arise from limited isolation of the antennas. It is shown that the system produces stable measurements of good quality and targeted corrected signals can be presented to the DUT in a limited amount of time. Overall these multi-port measurement showcase a proof-of-concept for the WB VNA based setup that will in future be expanded in BW as well as number of ports. The introduction of a directly synthesised source (DDS) will also enable improved triggering and absolute setting of each signal.

ACKNOWLEDGMENT

The work would not have been possible without the support from the group at Keysight Technologies working on the development and custom modification of the PNA-X platform including J. Dunsmore, T. Nielsen, J. Verspecht and J.-P. Teyssier. The authors would also like to thank the Microwave Engineering Center for Space Applications (MECSA) and WIN Semiconductors for providing access to the NP15-00 150-nm GaN-on-SiC process and the model used to design the DIDPA at UNIBO.

REFERENCES

[1] G. P. Gibiino, A. M. Angelotti, A. Santarelli, and P. A. Traverso, "Error vector magnitude measurement for power amplifiers under wideband load impedance mismatch: System-level analysis and vna-based implementation," *Measurement*, vol. 187, p. 110254, 2022.

[2] M. Mengozzi, G. P. Gibiino, A. M. Angelotti, A. Santarelli, C. Florian, and P. Colantonio, "Automatic optimization of input split and bias voltage in digitally controlled dual-input doherty rf pas," *Energies*, vol. 15, no. 13, p. 4892, 2022.

[3] O. Bengtsson, S. Paul, and C. Schulze, "A 26 ghz gan-mmic with integrated switches for discrete level supply modulation," in *IEEE MTT-S Int. Microw. Symp. Dig.*, 2021, pp. 527–530.

[4] N. Wolff, W. Heinrich, and O. Bengtsson, "Class-g supply modulation for mimo and radar with phased array antennas," in *Proc. German Microw. Conf.*, 2019.

[5] C. Nogales, L. Marzall, G. Lasser, and Z. Popović, "Dynamic supply modulation of a 6 – 12 ghz transmit array," in *IEEE Wireless and Microwave Technology Conf.*, 2023, pp. 140–143.

[6] "Scalable Performance Oscilloscopes, DPO70000SX Series Datasheet, Tektronix, 11 Apr 2023 55W 30662-27," Tektronik.

[7] "Infiniium UXR-B Series Oscilloscopes, Datasheet 3123-1313EN, Keysight Technologies, June 28, 2023," Keysight Technologies.
[8] S. Gustafsson, M. Thorsell, J. Stenarson, and C. Fager, "An oscilloscope correction method for vector-corrected rf measurements," *IEEE Trans. Instrum. Meas.*, vol. 64, no. 9, pp. 2541–2547, 2015.
[9] "RS FSW SIGNAL AND SPECTRUM ANALYZER - Continuing innovation in RF performance and usability, Product Brochure Version 14.00, Rohde und Schwarz, May 2023," Rohde und Schwarz.
[10] "Signal Analyzers X-Series, Product Brochure, 5992-1316EN, Keysight Technologies, March 16, 2023," Keysight Technologies.
[11] G. Avolio, G. Pailloncy, D. Schreurs, M. V. Bossche, and B. Nauwelaers, "On-wafer lsna measurements including dynamic-bias," in *Proc. European Microw. Conf.*, 2009, pp. 930–933.
[12] S. Gustafsson, M. Thorsell, K. Buisman, and C. Fager, "Vector-corrected nonlinear multi-port iq-mixer characterization using modulated signals," in *IEEE MTT-S Int. Microw. Symp. Dig.*, 2017, pp. 1433–1436.
[13] A. M. Angelotti, G. P. Gibiino, T. Nielsen, F. F. Tafuri, and A. Santarelli, "Three port non-linear characterization of power amplifiers under modulated excitations using a vector network analyzer platform," in *IEEE MTT-S Int. Microw. Symp. Dig.*, 2018, pp. 1021–1024.
[14] W. S. El-Deeb, N. Boulejfen, and F. M. Ghannouchi, "A multiport measurement system for complex distortion measurements of nonlinear microwave systems," *IEEE Trans. Instrum. Meas.*, vol. 59, no. 5, pp. 1406–1413, 2010.
[15] M. Litchfield, T. Reveyrand, and Z. Popović, "Load modulation measurements of x-band outphasing power amplifiers," *IEEE Trans. Microw. Theory Techn.*, vol. 63, no. 12, pp. 4119–4129, 2015.
[16] M. Marchetti, M. J. Pelk, K. Buisman, W. C. E. Neo, M. Spirito, and L. C. N. de Vreede, "Active harmonic load–pull with realistic wideband communications signals," *IEEE Trans. Microw. Theory Techn.*, vol. 56, no. 12, pp. 2979–2988, Dec. 2008.
[17] J. Verspecht, A. Stav, J. P. Teyssier, and S. Kusano, "Characterizing amplifier modulation distortion using a vector network analyzer," in *Proc. ARFTG Microw. Meas. Conf.*, 2019, pp. 1–4.
[18] A. M. Angelotti, G. P. Gibiino, C. Florian, and A. Santarelli, "Broadband error vector magnitude characterization of a gan power amplifier using a vector network analyzer," in *IEEE MTT-S Int. Microw. Symp. Dig.*, Jun. 2020.
[19] A. M. Angelotti, G. P. Gibiino, T. S. Nielsen, D. Schreurs, and A. Santarelli, "Wideband active load-pull by device output match compensation using a vector network analyzer," *IEEE Trans. Microw. Theory Techn.*, 2020.
[20] J. Verspecht, T. Nielsen, A. Stav, J. Dunsmore, and J.-P. Teyssier, "Modulation distortion analysis for mixers and frequency converters," in *Proc. ARFTG Microw. Meas. Conf.*, 2020, pp. 1–4.
[21] T. Niubó-Alemán, C. Liang, Y. Hahn, J. A. Reynoso-Hernández, J.-P. Teyssier, and P. Roblin, "Time-domain characterization and linearization of a dual-input power amplifier using a vector network analyzer as the receiver," *IEEE Trans. Microw. Theory Techn.*, vol. 69, no. 4, pp. 2386–2398, 2021.
[22] A. M. Angelotti, G. P. Gibiino, A. Santarelli, and P. A. Traverso, "Broadband measurement of error vector magnitude for microwave vector signal generators using a vector network analyzer," *IEEE Trans. Intrum. Meas.*, vol. 71, pp. 1–11, 2022.
[23] J. Verspecht, A. Stav, T. Nielsen, and S. Kusano, "The vector component analyzer: A new way to characterize distortions of modulated signals in high-frequency active devices," *IEEE Microw. Mag.*, vol. 23, no. 12, pp. 86–96, 2022.
[24] T. Niubó-Alemán *et al.*, "Calibrated digital predistortion using a vector network analyzer as the receiver," in *Proc. ARFTG Microw. Meas. Conf.*, 2019, pp. 1–4.
[25] W. Hallberg, D. Nopchinda, C. Fager, and K. Buisman, "Emulation of doherty amplifiers using single-amplifier load–pull measurements," *IEEE Microw. Wirel. Compon. Lett.*, vol. 30, no. 1, pp. 47–49, 2019.
[26] M. Mengozzi, G. P. Gibiino, A. M. Angelotti, C. Florian, A. Santarelli, C. Schulze, and O. Bengtsson, "Modulated-input control and linearization of a multi-port millimeter-wave pa by vna-based calibrated wideband measurements," in *Proc. ARFTG Microw. Meas. Conf.*, 2023, pp. 1–4.
[27] T. Wang, W. Li, R. Quaglia, and P. L. Gilabert, "Machine-learning assisted optimisation of free-parameters of a dual-input power amplifier for wideband applications," *Sensors*, vol. 21, no. 8, p. 2831, 2021.
[28] M. Mengozzi, A. M. Angelotti, G. P. Gibiino, C. Florian, and A. Santarelli, "Joint dual-input digital predistortion of supply-modulated rf pa by surrogate-based multi-objective optimization," *IEEE Transactions on Microwave Theory and Techniques*, vol. 70, no. 1, pp. 35–49, 2021.
[29] R. Darraji, F. M. Ghannouchi, and O. Hammi, "A dual-input digitally driven Doherty amplifier architecture for performance enhancement of Doherty transmitters," *IEEE Trans. Microw. Theory Techn.*, vol. 59, no. 5, pp. 1284–1293, 2011.
[30] C. Liang, P. Roblin, and Y. Hahn, "Accelerated design methodology for dual-input doherty power amplifiers," *IEEE Transactions on Microwave Theory and Techniques*, vol. 67, no. 10, pp. 3983–3995, 2019.
[31] A. Piacibello, R. Quaglia, V. Camarchia, C. Ramella, and M. Pirola, "Dual-input driving strategies for performance enhancement of a doherty power amplifier," in *Proc. IEEE MTT-S International Wireless Symp.*, 2018, pp. 1–4.
[32] J. Peng, W. Shi, J. Pang, F. You, and S. He, "Iterative learning control for signal separation in dual-rf input doherty transmitter," in *Proc.European Microw. Conf.*, 2021, pp. 953–956.
[33] H. Cao, J. Qureshi, T. Eriksson, C. Fager, and L. de Vreede, "Digital predistortion for dual-input doherty amplifiers," in *Proc. IEEE Topical Conf. on Power Amplifiers for Wireless and Radio Applications*, 2012, pp. 45–48.
[34] C. Kantana, R. Ma, M. Benosman, and Y. Komatsuzaki, "A Hybrid Heuristic Search Control Assisted Optimization of Dual-Input Doherty Power Amplifier," in *Proc. Eur. Microw. Conf.*, 2022, pp. 126–129.
[35] T. Reveyrand, A. Courty, M. Portelance, P. Medrel, P. Bouysse, and J.-M. Nébus, "Automatic vector signal generator calibration method suitable for multiport large-signal measurements," in *Proc. ARFTG Microw. Meas. Conf.*, 2019, pp. 1–4.
[36] "Low LO Drive Passive GaAs MMIC IQ Mixer - MMIQ-1040L datasheet," Marki Microwave.
[37] S. Laurent, J. P. Teyssier, R. Qúeré, J. Sombrin, and M. Prigent, "Linearity characterization of rf circuits through an unequally spaced multi-tone signal," in *Proc. ARFTG Microw. Meas. Conf.*, 2016, pp. 1–4.
[38] C. Schulze, W. Heinrich, J. Dunsmore, and O. Bengtsson, "Wideband vector corrected measurements on a modified vector network analyzer (vna) system," in *Proc. ARFTG Microw. Meas. Conf.*, 2022, pp. 1–4.
[39] M. Schroeder, "Synthesis of low-peak factor signals and binary sequences with low autocorrelation," *IEEE Transactions on Information Theory*, vol. 16, no. 1, pp. 85–89, 1970.
[40] J. Chani-Cahuana, P. N. Landin, C. Fager, and T. Eriksson, "Iterative learning control for rf power amplifier linearization," *IEEE Trans. Microw. Theory Techn.*, vol. 64, no. 9, pp. 2778–2789, 2016.

Christoph Schulze (Graduate Student Member, IEEE) received the B.Eng. degree in communication engineering from the HTW University of Applied Sciences Berlin, Germany, in 2014 and the M.Sc. degree in electrical engineering from the Technical University of Berlin, Germany, in 2018. Since 2020, he is with the Ferdinand-Braun-Institut gGmbH (FBH), Berlin Germany, where he currently holds the position of a scientific assistant. His research interests focus on MMIC power amplifier design and wideband modulated measurements on modified vector network analyzers.

Mattia Mengozzi (Graduate Student Member, IEEE) received the B.Sc. (2017) in computer engineering and the M.Sc. (2020) in electronic engineering at the University of Bologna. He is currently a Ph.D. student in Electronics, Telecommunications, and Information Technologies Engineering at the same university. His Ph.D. project focuses on microwave measurement techniques and performance optimization methods for high-efficiency 5G power amplifiers.

Gian Piero Gibiino (Member, IEEE) received the dual Ph.D. degree from the University of Bologna, Bologna, Italy, and KU Leuven, Leuven, Belgium, in 2016. He is currently an Assistant Professor with the Department of Electrical, Electronic, and Information Engineering "Guglielmo Marconi," University of Bologna. His main research interests include RF/microwave instrumentation and measurement, as well as measurement-based behavioral modeling and performance enhancement of RF/microwave devices and circuits. Dr. Gibiino is a member of the IEEE Microwave Theory and Techniques (MTT) and IEEE Instrumentation and Measurement (I&M) Societies, the Automatic Radio Frequency Techniques Group (ARFTG), the European Microwave Association (EuMA), and the Italian Association of Electrical and Electronic Measurements (GMEE). He is also an Affiliate Member of MTT TC-2 (design automation) and TC-3 (microwave measurements).

Alberto Maria Angelotti (Member, IEEE) received the Ph.D. degree in electronics, telecommunications, and information technology engineering from the University of Bologna, Bologna, Italy, in 2021. Since 2017, he has been with the Department of Electrical, Electronic, and Information Engineering "Guglielmo Marconi," University of Bologna, where he is currently a Post-Doctoral Research Fellow. His research interests include microwave instrumentation, nonlinear measurements, and characterization of gallium nitride devices, and power amplifiers.

Corrado Florian (Member, IEEE) received the Ph.D. degree in electronic and computer science engineering from the University of Bologna, Bologna, Italy, in 2004. He is currently Associate Professor of microwave electronics and power electronics with the Department of Electrical, Electronic and Information Engineering (DEI), University of Bologna. His research interests include microwave monolithic circuit design, hybrid RF circuit design, nonlinear dynamic circuits characterization and modelling, microwave device characterization and modelling, and power electronic circuits design.

Alberto Santarelli (Member, IEEE) received the Laurea degree (cum laude) in electronic engineering in 1991 and the Ph.D. in Electronics and Computer Science from the University of Bologna, Italy in 1996. He was a Research Assistant from 1996 to 2001 with the Research Centre for Computer Science and Communication Systems of the Italian National Research Council (IEIIT-CNR) in Bologna. In 2001, he joined the Department of Electrical, Electronic and Information Engineering "Guglielmo Marconi" (DEI), University of Bologna, where he currently is an Associate Professor. During his academic career he has been Lecturer of High-frequency Electronic Circuits, Applied Electronics and Power Electronics. His main research interests are related to nonlinear characterization and modeling of electron devices and to nonlinear circuit design. Prof. Santarelli is a member of the European Microwave Association (EuMA)..

Wolfgang Heinrich (Fellow, IEEE) received the PhD and Habilitation degrees in 1987 and 1992, respectively, from the Technical University of Darmstadt, Darmstadt, Germany. Since 1993, he has been with the Ferdinand-Braun-Institut (FBH) at Berlin, Germany, where he is the Head of the Microwave Department and the Deputy Scientific Director of the institute. Since 2008, he has been also Professor with the Technical University of Berlin. He has authored or coauthored more than 400 peer-reviewed publications and conference contributions. His present research interests include MMIC design with an emphasis on GaN and InP power amplifiers, as well as mm-wave and sub-mm-wave integrated circuits and packaging.

Olof Bengtsson (Senior Member, IEEE) received the B.Sc. degree in electrical engineering from the University of Gävle, Gävle, Sweden, in 1997, and the Lic.Tech. and Ph.D. degrees from the Department of Solid State Electronics (SSE), Ångström Laboratory, Uppsala University, Uppsala, Sweden, in 2006 and 2008, respectively. From 1998 to 2009, he was teaching microwave engineering at the University of Gävle. Since April 2009, he is with the Ferdinand-Braun-Institut (FBH), Berlin, Germany, where he currently holds the positions Head of the RF Power Lab and Group Leader for microwave measurements. His research interests include large-signal characterization of GaN devices for SISO and MIMO systems and the design of efficient discrete and integrated RF power amplifier systems based on load and supply modulation. Dr. Bengtsson is a member of the MTT-12 Microwave High-Power Techniques Committee since 2018.